



HAL
open science

Allosteric activation of *Bordetella pertussis* adenylyl cyclase by calmodulin: molecular dynamics and mutagenesis studies.

Edithe Selwa, Marilyne Davi, Alexandre Chenal, Ana-Cristina Sotomayor-Pérez, Daniel Ladant, Thérèse E Malliavin

► To cite this version:

Edithe Selwa, Marilyne Davi, Alexandre Chenal, Ana-Cristina Sotomayor-Pérez, Daniel Ladant, et al.. Allosteric activation of *Bordetella pertussis* adenylyl cyclase by calmodulin: molecular dynamics and mutagenesis studies.. *Journal of Biological Chemistry*, 2014, 289 (30), pp.21131-41. 10.1074/jbc.M113.530410 . pasteur-01107494

HAL Id: pasteur-01107494

<https://pasteur.hal.science/pasteur-01107494>

Submitted on 20 Jan 2015

HAL is a multi-disciplinary open access archive for the deposit and dissemination of scientific research documents, whether they are published or not. The documents may come from teaching and research institutions in France or abroad, or from public or private research centers.

L'archive ouverte pluridisciplinaire **HAL**, est destinée au dépôt et à la diffusion de documents scientifiques de niveau recherche, publiés ou non, émanant des établissements d'enseignement et de recherche français ou étrangers, des laboratoires publics ou privés.

June 5, 2014

Allosteric activation of *Bordetella pertussis* adenylyl cyclase by calmodulin: molecular dynamics and mutagenesis studies

Edithe Selwa^{1,3}, Marilynne Davi², Alexandre Chenal², Ana-Cristina Sotomayor-Pérez², Daniel Ladant^{*2} and Thérèse E Malliavin^{*1}

¹ Institut Pasteur and CNRS UMR 3528, rue du Dr Roux, Unité de Bioinformatique Structurale, 75015 Paris, France

² Institut Pasteur and CNRS UMR 3528, rue du Dr Roux, Unité de Biochimie des Interactions Macromoléculaires, 75015 Paris, France

³ Université Pierre et Marie Curie, Cellule Pasteur UPMC, rue du Dr Roux, 75015 Paris, France

Corresponding authors:

Thérèse E Malliavin, Unité de Bioinformatique Structurale, UMR CNRS 3528, rue du Dr Roux, 75015 Paris, France; mail: therese.malliavin@pasteur.fr, tel.: 00 33 1 45 68 88 54

Daniel Ladant, Unité de Biochimie des Interactions Macromoléculaires, UMR CNRS 3528, rue du Dr Roux, 75015 Paris, France; mail: daniel.ladant@pasteur.fr, tel.: 00 33 1 45 68 84 00

Keywords: adenylyl cyclase, *Bordetella pertussis*, calcium, calmodulin affinity, allostery, molecular dynamics

June 5, 2014

Running Title: AC mutants and AC/CaM interaction

Background: Adenylyl cyclase (AC) from *Bordetella pertussis* is activated when it interacts with calmodulin (CaM).

Results: A triple mutant of AC, which was predicted by molecular modeling, exhibited a highly reduced affinity for CaM.

Conclusion: This study suggests that a long-range connection between CaM and the AC catalytic loop is crucial for AC activation.

Significance: Molecular modeling identified critical molecular determinants for the allosteric activation of AC.

ABSTRACT

Adenylyl cyclase (AC) toxin is an essential toxin that allows *Bordetella pertussis* to invade eukaryotic cells, where it is activated after binding to calmodulin (CaM). Based on the crystal structure of the AC catalytic domain in complex with the C-terminal half of CaM (C-CaM), our previous molecular dynamics simulations (Selwa et al., *Proteins* 80, 1028–1040, 2012) suggested that three residues, i.e., Arg³³⁸,

Asn³⁴⁷, and Asp³⁶⁰, might be important for stabilizing the AC/CaM interaction. These residues belong to a loop-helix-loop motif (LHL) at the C-terminal end of AC, which is located at the interface between CaM and the AC catalytic loop. In the present study, we conducted the *in silico* and *in vitro* characterization of three AC variants, where one (Asn³⁴⁷; ACm1A), two (Arg³³⁸ and Asp³⁶⁰; ACm2A), or three residues (Arg³³⁸, Asn³⁴⁷, and Asp³⁶⁰; ACm3A) were substituted with Ala. Biochemical studies showed that the affinities of ACm1A and ACm2A for CaM were not affected significantly, whereas that of ACm3A was reduced dramatically. To understand the effects of these modifications, molecular dynamics (MD) simulations were performed based on the modified proteins. The MD trajectories recorded for the ACm3A/C-CaM complex showed that the calcium-binding loops of C-CaM exhibited large fluctuations, which could be related to the weakened interaction between ACm3A and its activator. Overall, our results suggest that the LHL motif at the C-terminal end of AC is crucial during CaM-binding for stabilizing the AC catalytic loop in an active configuration.

INTRODUCTION

The adenylyl cyclase toxin (CyaA) from *Bordetella pertussis*, the causative agent of whooping cough, plays an essential role in host invasion [1–3]. CyaA is able to invade eukaryotic target cells where it is activated by interacting with calmodulin (CaM), thereby overproducing cAMP, which disorganizes cellular signaling processes and triggers host cell death [4–12]. Several crystallographic structures have been reported of the CyaA catalytic domain (AC) in complex with the C terminal moiety of CaM

(C-CaM) [13] (Figure 1). These structures are physiologically relevant because C-CaM has been shown [14] to be as potent in activating the enzymatic activity of AC as the full-length CaM. In the AC/C-CaM complex (Figure 1a), the AC domain includes three main regions, CA (residues 7–61, 187–197, 261–299, and 313–345; colored in green) in the middle of the structure, and CB (residues 62–186, colored in orange) and SA (residues 192–254, colored in purple) at the two extremities. The C-terminal tail (residues 346–364, colored in cyan) and the C-loop of the catalytic site (residues 300–312, colored in yellow) are found in the CA region. At the C-terminal end of AC, a loop-helix-loop motif (LHL) that includes residues from Arg³³⁸ to Asp³⁶⁰ (Figure 1c) is present at the interface between C-CaM and a major AC catalytic loop that spans residues 300–312. In C-CaM, the calcium ions are bound to EF-hands 3 and 4, where EF-hand 3 is close to the interaction interface with AC.

In a previous study [15], we analyzed the interaction between the catalytic domain of AC from *B. pertussis* and C-CaM based on the molecular dynamics (MD) trajectories using maps of the energetic influences [16, 17]. Three residues in the LHL motif, i.e., Arg³³⁸, Asn³⁴⁷, and Asp³⁶⁰ (Figure 1b), were predicted to be important for the stability of the AC/CaM interaction, where Arg³³⁸ and Asp³⁶⁰ make contact with C-CaM, whereas Asn³⁴⁷ is in direct contact with the AC catalytic loop. In the present study, to further characterize the potential roles of these residues in AC/CaM interactions, we performed *in silico* MD simulations and *in vitro* biochemical and biophysical studies of the three modified AC proteins, where one (Asn³⁴⁷; ACm1A), two (Arg³³⁸ and Asp³⁶⁰; ACm2A), or three residues (Arg³³⁸, Asn³⁴⁷, and Asp³⁶⁰; ACm3A) were substituted with Ala. We found that the ACm3A variant exhibited a strongly reduced affinity for CaM, whereas the affinities of the ACm1A and ACm2A variants were similar to that of the wild-type enzyme.

This demonstrated the strong synergistic effects of the three mutations. The MD simulations showed that the differences in the behavior of the modified and wild-type complexes were related to differences in the internal mobility of the C-CaM calcium loops. These differences in mobility may induce direct or indirect weakening of the C-CaM/AC interaction observed in the ACm3A modified protein. These results, as well as an analysis of the geometrical strain, suggest that the LHL motif at the C-terminal end of AC is important for establishing a long-range connection between CaM binding and the stabilization of the AC catalytic loop in an active configuration, thus it is a critical module during the allosteric activation of AC by CaM.

1 EXPERIMENTAL PROCEDURES

MD simulations

The wild-type AC/C-CaM complexes in the presence (ACwt_2Ca) and absence (ACwt_0Ca) of calcium were prepared as described previously [15] and the three modified systems, i.e., ACm1A, ACm2A, and ACm3A, were generated in the following manner. The last snapshot of the simulation WT2Ca_T1 (see Table I for the definition of this trajectory) was extracted and the sidechains of the modified residues were replaced by Ala sidechains using the LEaP module from AMBER 10 [18] and the force field FF99SB [19]. Na⁺ counterions were added to neutralize the system.

The five systems, i.e., ACwt_2Ca, ACwt_0Ca, ACm1A, ACm2A, and ACm3A (Table I) were then hydrated in a box of TIP3P [20] water molecules using cutoff values of 10 or 12.5 Å and periodic boundary conditions. The calcium Lennard-Jones parameters of the Ca²⁺ ions comprised a van der Waals radius R of 1.7131 Å, and a well depth ϵ of 0.459789 kcal/mol [21].

The MD trajectories were initiated and ran as described previously [15]. For each sys-

tem, two simulations were recorded, which were labeled using the system name and the strings “T1” and “T2” (Table I).

The formation of hydrogen bonds between protein acceptor and donor groups was monitored by selecting donor and acceptor pairs with a proximity of less than 3 Å every ten recorded frames. This selection was implemented using the Biskit python library [22]. In the following, the AC and C-CaM residues are labeled based on their numbers in the crystallographic structure 1YRT [13] and the C-CaM residue numbers are followed by the letter *a*.

Along the MD trajectories, the geometric strain [23] of a residue *i* was calculated using the following equation:

$$p(i) = \sum_j (d_{ij} - \langle d_{ij} \rangle)^2 [1 - \tanh(\langle d_{ij} \rangle - 7)] / 2 \quad (1)$$

where $(d_{ij} - \langle d_{ij} \rangle)^2$ is the instantaneous deviation from the average of the distance d_{ij} between the α carbons of residues *i* and *j*. It was shown previously [23] that hinge residues are characterized by large $p(i)$ values.

Plasmids

Plasmid pTRAC384GK was used to express the wild-type AC (corresponding to the first 384 codons of CyaA, followed by the two residues Gly and Lys), as described previously [24]. Plasmids pKTRACm2A and pKTRACm3A, which were used to express ACm2A and ACm3A, respectively, were constructed from plasmid pKTRAC, an expression vector for the CyaC and CyaA proteins of *B. pertussis*. This plasmid was obtained from plasmid pTRACG [25] by replacing the ampicillin (Amp) resistance gene with a kanamycin (Kan) resistant gene from plasmid pKT25 [26]. In pKTRAC, both the *cyaC* and *cyaA* genes are expressed under the control of the λ phage Pr promoter. The plasmid has a ColE1 replication origin and it also expresses a thermosensitive λ repressor cI857, which strongly represses gene transcription at the λ Pr promoter at tempera-

tures below 32 °C. Thus, expression of the CyaC and CyaA proteins can be triggered by shifting the cells to 37–42 °C.

Plasmid pKTRACm3A was constructed by subcloning between the unique *AgeI* and *BamHI* sites of pKTRAC, a synthetic gene (synthesized by GeneArt, Life Technologies SAS, France) that encodes CyaA residues 320–384, followed by the two residues Gly and Lys, and where the three codons, Arg³³⁸, Asn³⁴⁷, and Asp³⁶⁰, were changed to Ala codons (the sequence of the ACm3A gene is available upon request).

Plasmid pKTRACm2A was constructed by subcloning between the unique *SnaBI* and *BsiWI* sites of plasmid pKTRACm3A using a double-stranded synthetic oligonucleotide produced via the hybridization of the following two oligonucleotides: 5'-GTTTTCTACGAAAACCGCGC-3' and 5'-GTACGCGCGGTTTTTCGTAGAAAAC-3' (Eurofins MWG GmbH, Ebersberg, Germany), thereby restoring the wild-type Asn³⁴⁷ codon (the *SnaBI* site was abolished after oligonucleotide insertion; see Figure S1). The DNA sequences of the modified *cyaA*' genes in pKTRACm2A and pKTRACm3A were confirmed by DNA sequencing (Eurofins MWG GmbH, Ebersberg, Germany).

Plasmid pKT7AC contained a synthetic AC gene (synthesized by GeneArt, Life Technologies SAS, France) that encoded the first 384 codons of CyaA, which was optimized for high expression in *Escherichia coli*, followed by the two residues Gly and Lys (the full DNA sequence is available upon request). This synthetic AC gene was cloned under the control of a T7 promoter and a synthetic RBS sequence in the vector pMK-RQ (GeneArt, Life Technologies SAS, France), a plasmid with a ColE1 replication origin and a Kan resistance gene.

Plasmid pKT7ACm1A was used to express ACm1A and it was constructed by subcloning between the unique *SnaBI* and *BsiWI* sites of plasmid pKT7AC, a double-stranded synthetic oligonucleotide, which was obtained

by hybridizing two oligonucleotides: 5'-GTGTTCTACGAAGCTCGCGC-3' and 5'-GTACGCGCGAGCTTCGTAGAACAC-3' (Eurofins MWG GmbH, Ebersberg, Germany), thereby replacing the wild-type Asn³⁴⁷ codon with an Ala codon (sequence available upon request). The DNA sequence of the modified *cyaA*' gene in pKT7ACm1A was confirmed by DNA sequencing (Eurofins MWG GmbH, Ebersberg, Germany).

Purification of AC proteins

The wild-type AC, ACm2A, and ACm3A were expressed in the *E. coli* BLR strain (Novagen, Darmstadt, Germany) by transformation with the plasmids pTRAC384GK, pKTRACm2A, and pKTRACm3A, respectively. The transformants were grown at 30 °C in LB medium that contained either 100 µg/mL Amp (for plasmid pTRAC384GK) or 50 µg/mL Kan (for plasmids pKTRACm2A or pKTRACm3A). When the culture reached an optical density of 0.6–0.8 at 600 nm, expression of the proteins was triggered by shifting the growth temperature to 42 °C. After 150 min of additional growth at 42 °C, the cells were collected by centrifugation (20 min, 10,000 × *g*, 4 °C) and the cell pellets were frozen at -20 °C.

ACm1A was expressed in the *E. coli* KRX strain (Promega, Madison, USA), which was transformed with the plasmid pKT7ACm1A. The transformants were grown at 37 °C in LB medium containing 50 µg/mL Kan to an optical density of 0.6–0.8. Next, expression of the proteins was triggered by the addition of 0.1% rhamnose (to induce the expression of the chromosomally encoded T7 RNA polymerase). After 180 min of additional growth at 37 °C, the cells were collected by centrifugation, as described above.

The cell pellets were resuspended in 20 mM HEPES-Na, pH 7.5, and disrupted by sonication at 4 °C. The sonicated suspension was centrifuged for 20 min at 13,000 × *g* and 4 °C. The supernatant was discarded

and the pellet was resuspended in 8 M urea with 20 mM HEPES-Na (pH 7.5), and agitated overnight at 4 °C. After 20 min of centrifugation at $13,000 \times g$ at 4 °C, the supernatant (“urea extract”) that contained the solubilized AC proteins was collected.

The AC proteins were purified according to a previously described protocol using two sequential chromatographic treatments with DEAE-Sepharose [24]. Briefly, the urea extract was first loaded onto a DEAE-Sepharose column (20 mL packed resin) equilibrated in 8 M urea with 20 mM HEPES-Na (pH 7.5). In these conditions, the AC protein did not bind to the resin and it was recovered in the flow-through (FT) fractions. The collected FT fractions were then diluted five times with 20 mM HEPES-Na (pH 7.5) and applied to a second DEAE-Sepharose column (20 mL packed resin), which had been equilibrated in 20 mM HEPES-Na (pH 7.5). In these conditions, the AC proteins were retained on the resin and, after extensive washing with 20 mM HEPES-Na (pH 7.5), the proteins were eluted in a soluble form using 20 mM HEPES-Na (pH 7.5) containing 100–200 mM NaCl. All of the AC protein preparations exceeded a purity of 95% according to SDS-PAGE analysis (Figure 6A). The AC protein content was determined based on the absorption spectra using an extinction coefficient at 278 nm of $28,000 \text{ M}^{-1}/\text{cm}^{-1}$.

AC enzymatic activity assays

The activity of AC was measured using a sensitive colorimetric assay, which was reported recently [27]. AC converts ATP into cAMP and pyrophosphate (PPi), and the latter can be hydrolyzed further by an exogenously added pyrophosphatase into two phosphate molecules (Pi), which can be quantified using a standard colorimetric assay based on the change in the absorbance of malachite green dye in the presence of phosphomolybdate complexes. The amount of Pi produced was determined using the Pi color Lock TM ALS colorimetric assay from

Innova Biosciences (Cambridge, UK).

The AC enzymatic assays were performed using a 96-well microtiter plate at 30°C in a final volume of 50 μL , which contained 50 mM Tris-HCl (pH 8.0), 10 mM MgCl_2 , 0.1 mM CaCl_2 , 0.5 mg/mL bovine serum albumin, 2 Unit/mL of *E. coli* inorganic pyrophosphatase (Sigma-Aldrich; the amount of pyrophosphatase added to the reaction medium was found to be sufficient to ensure the immediate and complete conversion of the released PPi into Pi), 0–1 μM of CaM, and 0.1–1 nM (depending on the specific activity) of AC proteins (diluted from stock solutions in 10 mM Tris-HCl with 0.2% Tween 20, pH 8.0). The mixtures were pre-incubated for 10 min at 30°C. Then, the enzymatic reactions were initiated by adding 2 mM ATP (final concentration) and the microplate was incubated at 30°C with agitation. At various incubation times (typically 2–10 min), 10 μL samples were taken from each well and transferred into a second 96-well microtiter plate, where each well contained 100 μL of a Pi-ALS mixture made of 2 volumes of H_2O plus 8 volumes of Pi ColorLock ALS reagent (provided in the Pi-ALS kit from Innova Biosciences). The enzymatic reaction was stopped immediately by the acidic conditions of the Pi-ALS mixture. After 10–13 min incubation at room temperature, 10 μL of stabilizer solution (from the Pi-ALS kit) was added to prevent further nonenzymatic breakdown of the phosphorylated substrate in acidic conditions (according to the kit instructions). After further incubation for 30–60 min at room temperature, the optical density at 595 nm (OD_{595}) was recorded using a microplate reader (Tecan, Lyon, France). A standard curve was obtained in parallel by adding known concentrations of Pi to the Pi-ALS mixture, which was used to convert the OD_{595} values into moles of PPi produced. The enzymatic activity was calculated based on the initial velocity of PPi synthesis (in the conditions described above, the accumulation of PPi was linear with time).

Biophysical characterization of AC proteins

Size exclusion chromatography (SEC) was performed using a Superdex 200 column (GE Healthcare), which was controlled by a GPCmax module that was connected online to a triple detector array (TDA) model 302 (Viscotek Ltd, Houston, Basingstoke, U.K.), as described previously [28]. The running buffer was buffer A (20 mM Hepes, 100 mM NaCl, pH 7.4) and the protein concentrations were 10–20 μM . Synchrotron radiation circular dichroism (SR-CD) experiments were conducted at the SOLEIL synchrotron facility (DISCO beamline, Gif-sur-Yvette, France), as described previously [29]. Briefly, the SR-CD spectra were recorded at 25°C using an integration time of 1.2 s and a bandwidth of 1 nm, with a 1-nm resolution step. Each far-UV spectrum represented the average of at least three individual scans. Optical cells with a 26 μm path-length and CaF_2 windows (Hellma) were used for recording CD signals in the far-UV region (180–260 nm). The protein concentrations were 25–50 μM for AC proteins and 250 μM for CaM in buffer A. Equimolar mixtures of enzyme and activator were used to obtain the AC-CaM and ACm3A-CaM spectra. The thermodynamic stability of the AC proteins was investigated by following their urea-induced denaturation (at 25°C, in buffer A), which was monitored by tryptophan fluorescence spectroscopy as described previously [30] using an FP-6200 spectrofluorimeter (Jasco, Japan) in a Peltier-thermostated cell holder, with a 1-cm path length quartz cell (101.QS, Hellma). The thermodynamic parameters (urea concentration required to unfold half the population of native proteins, $[\text{urea}]_{1/2}$, the cooperativity, m , and free energy, ΔG) were deduced from the fluorescence data, as described previously [30].

RESULTS

C-CaM/AC interface in the crystallographic structures

To explore the potential role of AC residues Arg³³⁸, Asn³⁴⁷, and Asp³⁶⁰ in CaM-induced activation, as suggested previously [15], we first checked the conservation of the atomic contacts established by these residues in the crystallographic structures of the AC/C-CaM complex [13]. The analysis of the hydrogen bonds and water-mediated contacts established between C-CaM and AC residues showed that the residues Arg³³⁸ and Asp³⁶⁰ were often involved in hydrogen bonds or in water-mediated contacts with C-CaM (data not shown, but available on request). Furthermore, most of the contacts and hydrogen bonds between the LHL motif (residues 338–360) (Figure 1c) and other AC residues were present in more than three crystallographic structures (data not shown, but available on request), thereby suggesting that the LHL motif plays an important role in the stabilization of the AC structure.

C-CaM/AC interaction along MD trajectories

Six independent MD simulations were recorded using the AC/C-CaM complex, where AC was modified in three different ways. Two simulations, i.e., "T1" and "T2," were performed for each AC variant, ACm1A (N347A), ACm2A (R338A, D360A), and ACm3A (R338A, N347A, D360A) (Figure 1b). The aim of these simulations was to analyze the relative stability of the different ACm/C-CaM complexes and to relate these to the observations described previously based on the X-ray crystallographic structures.

The conformational drift of the AC/C-CaM complex was monitored during trajectories ACm1A_T1, ACm2A_T1, ACm3A_T1, ACm1A_T2, ACm2A_T2, and ACm3A_T2 (Figure 2). The global RMSD calculated for the different AC/C-CaM complexes (Figures 2a and 2e) were similar

for all variants and they rapidly reached a plateau around 3 Å. The RMSD plateau was similar to that obtained based on the MD trajectories of the wild-type AC/C-CaM complex (Figure 2a in Ref [15]). Thus, these modifications did not destabilize the overall AC structure at least during the timescales considered by the MD trajectories.

The conformational drifts (RMSD) of the different protein regions in the two sets of simulations (Figures 2b-d and 2f-h) were very similar for CB (orange curves), the C loop (yellow curves), the F, G, H, and H' α helices, and the loop at the extremity of SA, which all had RMSD plateaus that were similar to or less than 2 Å. The CA region (green curves), SA region (violet curves), and C-terminal tail (cyan curves) had more significant drifts, where the RMSD values were larger than 4 Å. The CA and C terminal drifts are not surprising because the modified residues were located in these regions. Interestingly, the increased internal mobility of the C terminal tail is analogous to that observed in a wild-type AC/C-CaM complex (Figure 3a, b of Ref [15]) when the Ca^{2+} ions were removed (Figure 3a, b of Ref [15]). The latter had a lower affinity *in vitro*, thus the modifications of residues Arg³³⁸, Asn³⁴⁷, and Asp³⁶⁰ may have decreased the affinity of C-CaM for AC.

The water-mediated connections between AC and C-CaM were also analyzed along the MD trajectories (data not shown). The connections that involved the C-terminal tail of AC were present mainly in one or two trajectories, which shows that the interaction at this interface underwent reorganizations.

C-CaM and AC fluctuations in the MD trajectories

The behavior of C-CaM was monitored along the two series of mutant trajectories and compared with previous observations [15] obtained using the wild type AC/C-CaM complex.

In the simulation of the wild-type AC/C-CaM complex in the absence of calcium ions (WT0Ca_T1) (Figure 3a, solid red curve), the calcium loop of EF-hand 3 (i.e., between α helices V and VI) and the C-terminal part of α helix V exhibited highly increased fluctuations (RMSF). A similar increase was observed in ACm3A_T1 (Figure 3b, solid red curve) but in ACm2A_T2 and ACm3A_T2 (Figure 3b, dashed green and red curves), increased fluctuations were found in the calcium loop of EF-hand 4 (i.e., between α helices VII and VIII). Interestingly, the increased fluctuations in the C-terminal part of α helix V in ACm3A_T1 was associated with the small number of hydrogen bonds that connect C-CaM and C tail, i.e., only a single hydrogen bond is present for over 80% of the trajectory length between Arg^{90a} and Glu³⁴⁶.

Analysis of the internal fluctuations of AC along the various trajectories (data not shown) detected no major variations between the different modified proteins, which agreed with the similar global RMSD that was observed for all trajectories (Figure 2). The fluctuations measured in the wild-type systems were similar to those observed in the modified proteins, where the largest differences were observed for the 226–232 loop and the C-terminal tail of the protein. It should be noted that the loop 226–232 is not visible in the X-ray crystallographic structures, thereby indicating that it is probably a highly flexible region.

The coordination of calcium ions by the C-CaM residues was stable in the EF-hand 3 along the trajectories of the modified proteins (data available on request), but there were some variations in the EF-hand 4. Indeed, the calcium coordination by Asp¹³³ in the EF-hand 4 was perturbed in the two series of simulations. This perturbation agrees with the increased fluctuation observed in the calcium loop of EF-hand 4 for ACm2A_T2 and ACm3A_T2 (Figure 3b), and with the increase in the EF-hand 4 angle up to about 100°.

The C-CaM conformations were ex-

tracted from ACm2A_T2 and ACm3A_T2 (Figure 4) at times when different distances were observed between Asp¹³³-O δ 1/O δ 2 and the calcium ion. In both simulations, the sidechain of Asp¹³³ moved apart and at the end of the trajectory, the calcium ion was coordinated by the backbone carbonyl, instead of the sidechain. This conformational tendency of Asp¹³³ was increased in ACm3A_T2 compared with ACm2A_T2. Interestingly, in a steered MD study of the calcium dissociation in CaM [31], it was found that Asp¹³³ was among the latest residues to lose calcium coordination. The destabilization of the calcium/Asp¹³³ interaction observed in the present study corresponds to the destabilization of one of the strongest interactions that defines the calcium coordination in EF-hand 4. Thus, this destabilization indicates that the AC mutations decreased the calcium binding to CaM.

Overall, the perturbations of the EF-hand angles and calcium coordination are precursory indicators of the decrease in the C-CaM affinity for calcium ions [32,33]. On longer time scales, this decrease could lead to the dissociation of calcium ions from C-CaM and to a decrease in the affinity of AC for C-CaM, as shown previously [14].

Network of interactions involving LHL along the MD trajectories

The LHL motif, which contains the three modified residues, lies at the interface between C-CaM and the AC catalytic loop. The hydrogen bonds established by the residues in the LHL motif were analyzed in the different AC/C-CaM complexes (data available on request). Only long-range hydrogen bonds (that connected residues separated by more than ten residues in the protein sequence) were considered in order to exclude interactions related to local secondary structures. Most of these hydrogen bonds were conserved along the MD trajectories, except for one hydrogen bond between Asn³⁵ and Tyr³⁴², which was present only in the modified complexes, and two hy-

drogen bonds between Glu³⁴⁶ and Leu³⁵⁷, and between Tyr³⁵⁰ and Glu³⁰⁸, which were observed in less than two simulations. A lower number of stable hydrogen bonds that involved modified residues were observed in the ACm3A_T1 and ACm3A_T2 simulations. Indeed, Asn³⁴⁷ established hydrogen bonds with the residues Glu³⁰¹, Gln³⁰², and Asn³⁰⁴, which are located in the catalytic loop. These hydrogen bonds were disrupted by the change from Asn³⁴⁷ to Ala, except for the hydrogen bonds that involved the Asn³⁴⁷ backbone hydrogen. Similarly, the hydrogen bonds between Asp³⁶⁰ and Arg³³⁸ disappeared when Asp³⁶⁰ or Arg³³⁸ were modified to Ala. These observations show that the overall structure of the LHL motif is conserved in all systems, and that the LHL connection to C-CaM on one side, as well as to the C-loop on the other side, were significantly weakened in the presence of the triple modification.

The hydrogen bonds that involved LHL residues, as well as the protein fluctuations and the correlations in the fluctuation, indicated that there was limited variation among the protein variants (data not shown). Thus, the possibility of long-range communication through LHL was investigated using a parameter that was potentially more sensitive to small variations in geometry. The geometric strain, as defined by Chiappori et al. [23] (see Materials and Methods), exhibits sufficient sensitivity because it depends on the geometry of the environment of the analyzed residue within a sphere of 7 Å while it also follows the distance variations with respect to the average distance values.

The variations in the geometric strain along the MD trajectories exhibited correlated transitions between the given residues, which were due to simultaneous displacements of the environments of these residues. To summarize these variations, the time correlation matrices of the geometric strain were analyzed. The strain correlation peaks (in pink/yellow) correspond to residue pairs that are undergoing correlated displace-

ments in their environment, thus they are mechanically correlated. In order to estimate the reliability of the correlation predictions, the calculation was repeated five times by selecting at each time, one data-point over five along the analyzed time interval. The average values were calculated among LHL residues (Figure 5) and among the LHL, C-loop and calcium loop residues (data not shown but available on request). The standard deviations obtained from the repeated calculation of the correlations allowed us to estimate the error on the correlation, which was 4–6.5% for correlations greater than 0.15. In all trajectories, the peaks were observed repeatedly between residues in the α -helix at 346–355. A general attenuation of the correlations, with pixel colors changing from pink to yellow, was observed for the trajectories recorded in the protein variants compared with those recorded in the wild type. This suggests that there was a decrease in the long-range correlation along the LHL for the modified proteins.

In vitro characterization of AC variants that harbored mutations at positions 338, 347 or 360

To further delineate the effect of the mutations on the activity of AC and its affinity for CaM, the three variants ACm1A, ACm2A, and ACm3A were characterized *in vitro* (see Materials and Methods). The three modified proteins and the wild-type catalytic domain (AC) were overexpressed in *E. coli* and purified to homogeneity, as described previously ([24], see Materials and Methods). The results of the SDS-PAGE analysis of the purified preparations are shown in Figure 6A.

The enzymatic activities of each AC variant were determined at different CaM concentrations, which ranged from 0.03 nM to 1 μ M. Figure 6B shows the CaM-dependency of the enzymatic activity for each variant as a percentage of the maximal activity (100 %) determined at the saturat-

ing CaM concentration of 1 μ M. The affinities of the AC enzymes for CaM, which were defined as the CaM concentration at half-maximal activation $K_{1/2}$, were determined (Figure 6C) by curve-fitting with a single binding isotherm, according to $A = A_{Max} (C/C + K_{1/2})$ where C is the concentration of CaM, A is the activity at the concentration C of CaM, and A_{Max} is the maximal activity measured in the presence of 1 μ M CaM.

As shown in Figures 6B and C, wild-type AC (labeled AC_{WT} in Figure 6C) exhibited a k_{cat} of 4600 s⁻¹ (at saturating CaM and 2 mM ATP) and a half-maximal CaM activation $K_{1/2}$ of 0.11 nM, which agreed well with previous studies [13, 24, 34]. The ACm1A variant, where the Asn³⁴⁷ residue that interacted with the catalytic loop was modified to Ala, exhibited an enzymatic activity that was reduced by about half ($k_{cat} \sim 2250$ s⁻¹) compared with the wild type and a \sim five-fold lower affinity for CaM ($K_{1/2}^{CaM}$ of 0.61 nM). The dual mutations R338A and D360A in the ACm2A variant did not affect the catalytic efficiency ($k_{cat} \sim 6000$ s⁻¹ was even slightly higher than that of the wild type) but the affinity for CaM was reduced by about six-fold ($K_{1/2}^{CaM}$ of 0.66 nM), as might be expected with modifications at the CaM interface. Finally, the triple mutant ACm3A was the enzyme that was affected most significantly, where its catalytic turnover ($k_{cat} \sim 650$ s⁻¹) was decreased significantly compared with the wild-type AC (ca 15% of the wild type turnover) and its affinity for CaM ($K_{1/2}^{CaM}$ of 26 nM) was reduced by more than 200 times.

These data indicate that the separate single (N347A) and dual (R338A, and D360A) modifications had limited effects on the catalytic and CaM-binding properties of AC, whereas their combination in a single enzyme (ACm3A) had strong synergistic effects on both the enzymatic activity and the affinity for CaM. This fully supports our prediction that the LHL region is critical for the allosteric coupling of CaM binding to the stabilization of the catalytic loop in an enzy-

matically active configuration. The two- to five-fold higher K_M^{ATP} levels of all the modified AC enzymes compared with the wild-type AC also demonstrate that the LHL motif is important for maintaining the optimal conformation of the active site.

To verify that the triple modification of R338A, N347A, and D360A in ACm3A did not affect the structural integrity of the protein, we performed the following biophysical analyses. First, the proteins were analyzed by SEC followed by triple detector array (SEC-TDA) to determine whether the mutations affected their oligomeric status. SEC-TDA provides the molecular masses of the eluted species by combining static right angle light scattering with UV absorbance. The results showed that both the wild-type and ACm3A proteins were monomeric species in solution (Figure 7A). The secondary structure contents of the CaM and AC proteins, either isolated or in complexes, were analyzed by SRCD in the far-UV range. The shapes of the far-UV CD spectra of wild-type AC and ACm3A were similar (Figure 7B). The addition of CaM induced similar changes in the overall secondary structure content of both AC proteins. These results clearly indicate that the secondary structure content of ACm3A was not affected by the mutations. Finally, the thermodynamic stability of both AC proteins was characterized. The urea-induced denaturation of the AC proteins was monitored by tryptophan fluorescence. The denaturation profiles (Figure 7C). and the thermodynamic parameters (Figure 7D) obtained for both proteins were very similar. Overall, these experiments indicate that the three modifications in ACm3A did not affect the structural properties or the overall stability of the protein.

DISCUSSION

Maps of the energetic influences [16, 17] that were calculated [15] previously using the AC/C-CaM complex allowed us to identify three residues, i.e., Arg³³⁸, Asn³⁴⁷, and

Asp³⁶⁰, that might affect the interaction between AC and C-CaM. In the present study, we characterized three modified proteins, i.e., ACm1A (N347A), ACm2A (R338A, D360A), and ACm3A (R338A, N347A and D360A), using *in silico* MD simulations and based on *in vitro* biochemical and biophysical studies.

Our *in vitro* studies showed that the affinity of the triple mutant ACm3A for CaM was greatly reduced whereas that of the single (ACm1A) or dual mutant (ACm2A) was not affected significantly compared with that of the wild-type enzyme. These results indicate that these three mutations had a strong synergistic effect on the CaM-binding affinity. A similar synergistic effect was noted for the catalytic efficiency of the enzyme because the enzymatic activity of ACm3A was also reduced significantly (about 15% of the wild-type enzyme activity), whereas that of ACm1A was about 50% of the wild-type activity. The lower activity of the ACm1A and ACm3A variants might be expected because the Asn³⁴⁷ residue interacts directly with the catalytic loop. Thus, any perturbation of the interaction between Asn³⁴⁷ and the catalytic loop might directly affect the catalytic efficiency of AC.

The dynamical behaviors of the three modified proteins in complex with C-CaM were also analyzed *in silico* based on two series of MD simulations. High variability in the establishment of hydrogen bonds in the complex was observed in the different modified proteins, as well as among repeated trajectories. However, this variability could not be assigned to simulation artifacts because similar variability was observed among the four crystallographic structures of the complex AC/C-CaM [13]. The analysis of the trajectories recorded using modified and wild-type AC/C-CaM complexes, which were conducted in parallel with the experimental characterization of the AC/CaM interaction, identified two different routes that allowed the affinity of AC for C-CaM to decrease. In the first

simulation of the triple modified protein (ACm3A_T1), a destabilization of the calcium loop of EF-hand 3 was observed, as well as a large decrease in the interactions between C-CaM and the CA region. In the second trajectory recorded using ACm3A (ACm3A_T2), a destabilization of the calcium coordination in the EF-hand 4 of C-CaM led to the disruption of the hydrogen bond between the Asp¹³³ sidechain and calcium. This could be the first step in the possible dissociation of calcium from C-CaM. It is known that calcium-free CaM has a lower affinity for AC [14], thus the destabilization of calcium coordination would result in a reduction of the CaM affinity for AC.

Guo et al. [13] described the crystallographic structure of the complex AC/C-CaM and characterized one AC modification: the double modification E346A/R348A in the C terminal tail. The modified protein exhibited a reduced enzymatic activity as well as a reduced affinity for CaM. The two amino acids changed in the E346A/R348A mutant flanked the Asn³⁴⁷ residue that was modified in the present study. The hydrogen bonds that involve Glu³⁴⁶ and Arg³⁴⁸ residues varied in the wild-type AC when calcium ions or C-CaM were removed from the system, as well as in the trajectories of the modified AC protein, but no systematic variations were detected. However, the observations of Guo et al. [13] based on the E346A/R348A AC variant agree well with our present study, as well as supporting the hypothesis that the LHL motif is critical for linking CaM binding with the stabilization of the AC catalytic loop in a configuration that is favorable for catalysis. Indeed, the LHL motif is in direct contact with C-CaM on one side via the Arg³³⁸ and Asp³⁶⁰ residues, as well as the catalytic loop on the other side via the Asn³⁴⁷ residue. Thus, it is ideally positioned to relay information related to CaM-binding on the distant catalytic site of the AC enzyme via a dense network of atomic contacts, which primarily involve the Arg³³⁸, Asn³⁴⁷, and Asp³⁶⁰

residues, as demonstrated in our MD simulations. Long-range communications within the LHL motif were further suggested by our analysis of the geometric strain along the MD trajectories of the different ACs. Therefore, the LHL motif appears to be a critical module for the allosteric activation of AC by CaM. The analysis performed in the present study was more qualitative than the method proposed recently by Weinkam et al. [35,36], but we should note that the availability of only one structure of AC in complex with Ca²⁺-loaded C-CaM, as well as the conformational equilibrium that is probably adopted by AC in the unbound state, prevent a more straightforward application of this method.

From a more general perspective, the detection of the residue networks that are responsible for long-range communication inside a given protein has been attracting much interest during the last decade [37–41]. These networks are thought to be involved in biomolecular interactions [42] with fundamental roles in many biological processes [43]. Homologous protein sequence alignments [44–46] or analysis of the covariance of the NMR chemical shifts [47] have predicted long-range protein communication networks that agree with experimental observations. Some of these analyses have facilitated protein engineering [48]. In the present study, we combined MD and mutagenesis to identify a long-range communication network related to the activation of a key virulence factor derived from a bacterial pathogen. This investigation may facilitate new methods for interfering with the AC-CaM interaction, thereby allowing a novel drug discovery approach [49].

ACKNOWLEDGMENTS

We acknowledge SOLEIL for providing the synchrotron radiation facilities (Proposal IDs 20110586 and 20120444) and we thank Frank Wien for assistance with using the DISCO beamline. Edithe Selwa was supported by an allocation doctorale from

MENRT, which was distributed by Université Pierre et Marie Curie (Paris VI). Ana Cristina Sotomayor Pérez was supported by an Institut Pasteur PTR grant (PTR#374). This project was supported by the Institut Pasteur and the Centre National de la Recherche Scientifique (CNRS UMR 3528, Biologie Structurale et Agents Infectieux). Data not shown in the manuscript may be obtained from the authors (Daniel Ladant: daniel.ladant@pasteur.fr; Thérèse Malliavin: therese.malliavin@pasteur.fr) on request.

References

- [1] Ladant, D. and Ullmann, A. (1999) Bordetella pertussis adenylate cyclase: a toxin with multiple talents. *Trends Microbiol* **7**, 172–176
- [2] Vojtova, J., Kamanova, J., and Sebo, P. (2006) Bordetella adenylate cyclase toxin: a swift saboteur of host defense. *Curr Opin Microbiol* **9**, 69–75
- [3] Carbonetti, N. (2010) Pertussis toxin and adenylate cyclase toxin: key virulence factors of Bordetella pertussis and cell biology tools. *Future Microbiol* **5**, 455–469
- [4] Wolff, J., Cook, G., Goldhammer, A., and Berkowitz, S. (1980) Calmodulin activates prokaryotic adenylate cyclase. *Proc Natl Acad Sci USA* **77**, 3841–3844
- [5] Confer, D. and Eaton, J. (1982) Phagocyte impotence caused by an invasive bacterial adenylate cyclase. *Science* **217**, 948–950
- [6] Rogel, A., Schultz, J., Brownlie, R., Coote, J., Parton, R., and Hanski, E. (1989) Bordetella pertussis adenylate cyclase: purification and characterization of the toxic form of the enzyme. *EMBO J* **8**, 2755–2760
- [7] Goodwin, M. and Weiss, A. (1990) Adenylate cyclase toxin is critical for colonization and pertussis toxin is critical for lethal infection by Bordetella pertussis in infant mice. *Infect Immun* **58**, 3445–3447
- [8] Khelef, N., Zychlinsky, A., and Guiso, N. (1993) Bordetella pertussis induces apoptosis in macrophages: role of adenylate cyclase-hemolysin. *Infect Immun* **61**, 4064–4071
- [9] Harvill, E., Cotter, P., Yuk, M., and Miller, J. (1999) Probing the function of Bordetella bronchiseptica adenylate cyclase toxin by manipulating host immunity. *Infect Immun* **67**, 1493–1500
- [10] Hewlett, E., Donato, G., and Gray, M. (2006) Macrophage cytotoxicity produced by adenylate cyclase toxin from Bordetella pertussis: more than just making cyclic AMP! *Mol Mic* **59**, 447–459
- [11] Cheung, G., Dickinson, P., Sing, G., Craigon, M., Ghazal, P., Parton, R., and Coote, J. (2008) Transcriptional responses of murine macrophages to the adenylate cyclase toxin of Bordetella pertussis. *Microb Pathog* **44**, 61–70
- [12] Kamanova, J., Kofronova, O., Masin, J., Genth, H., Vojtova, J., Linhartova, I., Benada, O., Just, I., and Sebo, P. (2008) Adenylate cyclase toxin subverts phagocyte function by RhoA inhibition and unproductive ruffling. *J Immunol* **181**, 5587–5597

- [13] Guo, Q., Shen, Y., Lee, Y., Gibbs, C., Mrksich, M., and Tang, W. (2005) Structural basis for the interaction of *Bordetella pertussis* adenylyl cyclase toxin with calmodulin. *EMBO J.* **24**, 3190–3201
- [14] Shen, Y., Lee, Y., Soelaiman, S., Bergson, P., Lu, D., Chen, A., Beckingham, K., Grabarek, Z., Mrksich, M., and Tang, W. (2002) Physiological calcium concentrations regulate calmodulin binding and catalysis of adenylyl cyclase exotoxins. *EMBO J.* **21**, 6721–6732
- [15] Selwa, E., Laine, E., and Malliavin, T. (2012) Differential role of Calmodulin and Calcium ions in the stabilization of the catalytic domain of adenylyl cyclase CyaA from *Bordetella pertussis*. *Proteins* **80**, 1028–1040
- [16] Hamacher, K., Trylska, J., and McCammon, J. (2006) Dependency map of proteins in the small ribosomal subunit. *PloS Comput. Biol.* **2**, e10
- [17] Laine, E., Blondel, A., and Malliavin, T. (2009) Dynamics and Energetics: A Consensus Analysis of the Impact of Calcium on EF-CaM Protein Complex. *Biophysical Journal* **96**, 1–15
- [18] Case, D., Cheatham, T., Darden, T., Gohlke, H., Luo, R., Merz, K., Onufriev, A., Simmerling, C., Wang, B., and Woods, R. (2005) The AMBER biomolecular simulation programs. *J Computat Chem* **26**, 1668–1688
- [19] Hornak, V., Abel, R., Okur, A., Strockbine, B., Roitberg, A., and Simmerling, C. (2006) Comparison of multiple AMBER force fields and development of improved protein backbone parameters. *Proteins* **65**, 712–725
- [20] Jorgensen, W. (1981) Transferable intermolecular potential functions for water, alcohols and ethers. application to liquid water. *J. Am. Chem. Soc.* **103**, 335–340
- [21] Aqvist, J. (1990) Ion-water interaction potentials derived from free energy perturbation simulations. *J Phys Chem* **94**, 8021–8024
- [22] Grunberg, R., Nilges, M., and Leckner, J. (2007) Biskit—a software platform for structural bioinformatics. *Bioinformatics* **23**, 769–770
- [23] Chiappori, F., Merelli, I., Colombo, G., Milanese, L., and Morra, G. (2012) Molecular mechanism of allosteric communication in Hsp70 revealed by molecular dynamics simulations. *PLoS Comput Biol* **8**, e1002844
- [24] Vouquier, S., Mary, J., Dautin, N., Vinh, J., Friguet, B., and Ladant, D. (2004) Essential role of methionine residues in calmodulin binding to *Bordetella pertussis* adenylyl cyclase, as probed by selective oxidation and repair by the peptide methionine sulfoxide reductases. *J Biol Chem* **279**, 30210–30218
- [25] Gmira, S., Karimova, G., and Ladant, D. (2001) Characterization of recombinant *Bordetella pertussis* adenylyl cyclase toxins carrying passenger proteins. *Research in microbiology* **152**, 889–900
- [26] Karimova, G., Ullmann, A., and Ladant, D. (2001) Protein-protein interaction between *Bacillus stearothermophilus* tyrosyl-tRNA synthetase subdomains revealed by a bacterial two-hybrid system. *Journal of molecular microbiology and biotechnology* **3**, 73–82

- [27] Laine, E., Goncalves, C., Karst, J., Lesnard, A., Rault, S., Tang, W., Malliavin, T., Ladant, D., and Blondel, A. (2010) Use of allostery to identify inhibitors of calmodulin-induced activation of Bacillus anthracis Edema Factor. *Proc. Natl. Acad. Sci. U.S.A.* **107**, 11277–11282
- [28] Karst, J., Sotomayor-Pérez, A., Guijarro, J., Raynal, B., Chenal, A., and Ladant, D. (2010) Calmodulin-induced conformational and hydrodynamic changes in the catalytic domain of Bordetella pertussis adenylate cyclase toxin. *Biochemistry* **49**, 318–328
- [29] Sotomayor-Pérez, A., Subrini, O., Hessel, A., Ladant, D., and Chenal, A. (2013) Molecular Crowding Stabilizes Both the Intrinsically Disordered Calcium-Free State and the Folded Calcium-Bound State of a Repeat in Toxin (RTX) Protein. *J Am Chem Soc* **135**, 11929–11934
- [30] Chenal, A., Karst, J., Sotomayor-Pérez, A., Wozniak, A., Baron, B., England, P., and Ladant, D. (2010) Calcium-induced folding and stabilization of the intrinsically disordered RTX domain of the CyaA toxin. *Biophys J* **99**, 3744–3753
- [31] Zhang, Y., Tan, H., Lu, Y., Jia, Z., and Cheng, G. (2008) Ca(2+) dissociation from the C-terminal EF-hand pair in calmodulin: a steered molecular dynamics study. *FEBS Lett* **582**, 1355–1361
- [32] Zhang, M., Tanaka, T., and Ikura, M. (1995) Calcium-induced conformational transition revealed by the solution structure of apo calmodulin. *Nat Struct Biol* **2**, 758–767
- [33] Finn, B., Evenas, J., Drakenberg, T., Waltho, J., Thulin, E., and Forsen, S. (1995) Calcium-induced structural changes and domain autonomy in calmodulin. *Nat Struct Biol* **2**, 777–783
- [34] Glaser, P., Elmaoglou-Lazaridou, A., Krin, E., Ladant, D., Bárzu, O., and Danchin, A. (1989) Identification of residues essential for catalysis and binding of calmodulin in Bordetella pertussis adenylate cyclase by site-directed mutagenesis. *EMBO J* **8**, 967–972
- [35] Weinkam, P., Pons, J., and Sali, A. (2012) Structure-based model of allostery predicts coupling between distant sites. *PNAS* **109**, 4875–4880
- [36] Weinkam, P., Chen, Y., Pons, J., and Sali, A. (2013) Impact of mutations on the allosteric conformational equilibrium. *J Mol Biol* **425**, 647–661
- [37] Chennubhotla, C. and Bahar, I. (2007) Signal propagation in proteins and relation to equilibrium fluctuations. *PLoS Comput Biol* **3**, 1716–1726
- [38] del Sol, A., Tsai, C., Ma, B., and Nussinov, R. (2009) The origin of allosteric functional modulation: multiple pre-existing pathways. *Structure* **17**, 1042–1050
- [39] Dubay, K., Bothma, J., and Geissler, P. (2011) Long-range intra-protein communication can be transmitted by correlated side-chain fluctuations alone. *PLoS Comput Biol* **7**, e1002168
- [40] Kuzu, G., Keskin, O., Gursoy, A., and Nussinov, R. (2012) Constructing structural networks of signaling pathways on the proteome scale. *Curr Opin Struct Biol* **22**, 367–377

- [41] Cilia, E., Vuister, G., and Lenaerts, T. (2012) Accurate prediction of the dynamical changes within the second PDZ domain of PTP1e. *PLoS Comput Biol* **8**, e1002794
- [42] Bakan, A. and Bahar, I. (2009) The intrinsic dynamics of enzymes plays a dominant role in determining the structural changes induced upon inhibitor binding. *Proc Natl Acad Sci USA* **106**, 14349–14354
- [43] Nussinov, R., Ma, B., Tsai, C., and Csermely, P. (2013) Allosteric conformational barcodes direct signaling in the cell. *Structure* **21**, 1509–1521
- [44] Lockless, S. and Ranganathan, R. (1999) Evolutionarily conserved pathways of energetic connectivity in protein families. *Science* **286**, 295–299
- [45] Dickson, R., Wahl, L., Fernandes, A., and Gloor, G. (2010) Identifying and seeing beyond multiple sequence alignment errors using intra-molecular protein covariation. *PLoS One* **5**, e11082
- [46] Reynolds, K., McLaughlin, R., and Ranganathan, R. (2011) Hot spots for allosteric regulation on protein surfaces. *Cell* **147**, 1564–1575
- [47] Selvaratnam, R., Chowdhury, S., VanSchouwen, B., and Melacini, G. (2011) Mapping allostery through the covariance analysis of NMR chemical shifts. *Proc Natl Acad Sci U S A* **108**, 6133–6138
- [48] Lee, J., Natarajan, M., Nashine, V., Socolich, M., Vo, T., Russ, W., Benkovic, S., and Ranganathan, R. (2008) Surface sites for engineering allosteric control in proteins. *Science* **322**, 438–442
- [49] Seifert, R. and Dove, S. (2012) Towards selective inhibitors of adenylyl cyclase toxin from *Bordetella pertussis*. *Trends Microbiol* **20**, 343–351
- [50] Eswar, N., Eramian, D., Webb, B., Shen, M., and Sali, A. (2008) Protein structure modeling with MODELLER. *Methods Mol Biol* **426**, 145–159

FIGURE LEGENDS

Figure 1

a) X-ray crystallographic structure of the catalytic domain (AC) of adenylyl cyclase (CyaA, PDB entry 1YRT) drawn in cartoons. Helices F, G, and H colored in purple form the SA region (residues 192–254). The loop 226–232 (Hom loop) colored in salmon at the left extremity of SA colored in purple was missing from the X-ray crystallographic structure and was modeled using Modeller9v4 [50]. The other protein regions are colored in green (CA: residues 7–61, 187–197, 261–299, and 313–345), orange (CB: residues 62–186), cyan (C-terminal tail/C tail: residues 346–364), and yellow (catalytic loop/C loop: residues 300–312). The C-CaM lobe, which is colored in red, interacts with SA and the C-terminal tail. Calcium ions are represented by silver beads. b) The modified residues, i.e., Arg³³⁸, Asn³⁴⁷, and Asp³⁶⁰, located in CA and the C terminal tail, are indicated by sticks. c) The LHL motif localized between the C-CaM/AC interface and the catalytic loop is colored in brown.

Figure 2

Conformational drifts estimated based on the α carbon coordinates RMSD from the starting conformations in the T1 (a-d) and T2 (e-h) series of simulations. (a, e) Drift calculated based on the C α carbons in the AC domain for ACm1A (black), ACm2A (green), and ACm3A (red). (b–d, f–h) Drift calculated based on different regions of the AC domain, which were analyzed for ACm1A (b, f), ACm2A (c, g), and ACm3A (d, h). The color codes of the different protein regions are shown in panel (d). The AC regions are defined as follows. 1) CA: residues 7–61, 187–197, 261–299, and 313–345. 2) Catalytic loop (C Loop): residues 300–312. 3) C-terminal tail (C tail): residues 346–364. 4) CB: residues 62–186. 5) SA: residues 198–260. Helices H, F, G, and H' correspond to residues 234–253, 198–210, 214–223, 256–260.

Figure 3

Fluctuations of the residues (RMSF: Å) observed in C-CaM based on the trajectories recorded for: (a) wild-type and (b) modified C-CaM/AC complexes. The trajectory names are shown in the legends. The WT2Ca trajectories were run on two Ca²⁺-loaded AC/C-CaM complexes, whereas the WT0Ca trajectories were run on the AC/C-CaM complex in the absence of calcium ions. The fluctuations were calculated based on the trajectories after removing their first 10 ns.

Figure 4

C-CaM conformation extracted from ACm2A_T2 and ACm3A_T2, which are colored according to the simulation times indicated. The N- and C-terminal ends are indicated, as well as Asp-133, which is shown in black. The calcium ions are shown as gray spheres, and the carboxyl oxygens of the Asp-133 sidechain are colored in red.

Figure 5

Correlation between geometric strains among the LHL residues, displayed for each recorded trajectory. The time-correlation matrices were calculated between the variations of the geometric strains of LHL residues and the first ten nanoseconds were discarded from the analysis. In order to estimate the reliability of the prediction of correlation, the calculation was repeated five times by selecting at each time, one data-point over five along the analyzed time interval. The average values calculated for the LHL residues are shown

in the figure. The intensity scale varies from 1.0 (pink) to -0.2 (dark green).

Figure 6

A. SDS-PAGE analysis of the purified AC variants, wild type AC, and CaM. The proteins were separated by electrophoresis on a 4–12% SDS-polyacrylamide gel (Life Technologies). After migration, the gel was stained with PageBlue protein staining solution (Thermo Fisher Scientific). B. Activation of modified ACs by CaM. The activity of the purified wild-type AC and/or the variants were measured (as described in the Materials and Methods) in the presence of the indicated CaM concentrations, and the results are expressed as the percentage of the maximal activity (measured in the presence of $1\mu\text{M}$ CaM). C. Catalytic properties of AC variants. The parameters were determined within an error of $\pm 10\%$. ΔG is the calculated energy of association between CaM and AC.

Figure 7

A. SEC-TDA analysis of the oligomerization state of ACwt and ACm3A. Red curve: right angle light scattering; blue curve: UV absorbance; green curve: molecular masses of the eluted species. See the Materials and Methods for details. B. Synchrotron radiation circular dichroism spectra of CaM and AC proteins in isolation or in a 1:1 complex. MRE: mean residual ellipticity. See the Materials and Methods for details. C. Thermodynamic stability of AC proteins following urea-induced denaturation. The ratio of the fluorescence intensity at 360 and 320 nm (excitation wavelength = 295 nm) for the proteins as a function of the urea concentration was measured as described in the Materials and Methods. D. Thermodynamics parameters of the urea-induced denaturation of AC proteins.

Table I **Details of the molecular systems simulated in molecular dynamics (MD) trajectories.**

Systems	ACwt_2Ca	ACwt_0Ca
Trajectories	WT2Ca_T1 WT2Ca_T2	WT0Ca_T1 WT0Ca_T2
Number of Na ⁺ counter-ions	14	18
Water box dimensions	92.6 x 106.9 x 103.3 Å ³	91.3 x 106.9 x 106.4 Å ³
Number of water molecules	26455	27056
Total number of atoms	85825	87630
Length (ns)	30	30

Table I

Systems	ACm1A	ACm2A	ACm3A
Trajectories	ACm1A_T1 ACm1A_T2	ACm2A_T1 ACm2A_T2	ACm3A_T1 ACm3A_T2
Number of Na ⁺ counter-ions	14	18	14
Water box dimensions	109.6 x 82.8 x 111.7 Å ³	108.1 x 82.8 x 111.7 Å ³	109.6 x 82.8 x 111.7 Å ³
Number of water molecules	29003	29008	29008
Total number of atoms	93465	93468	93464
Length (ns)	50	50	50

Figure 1

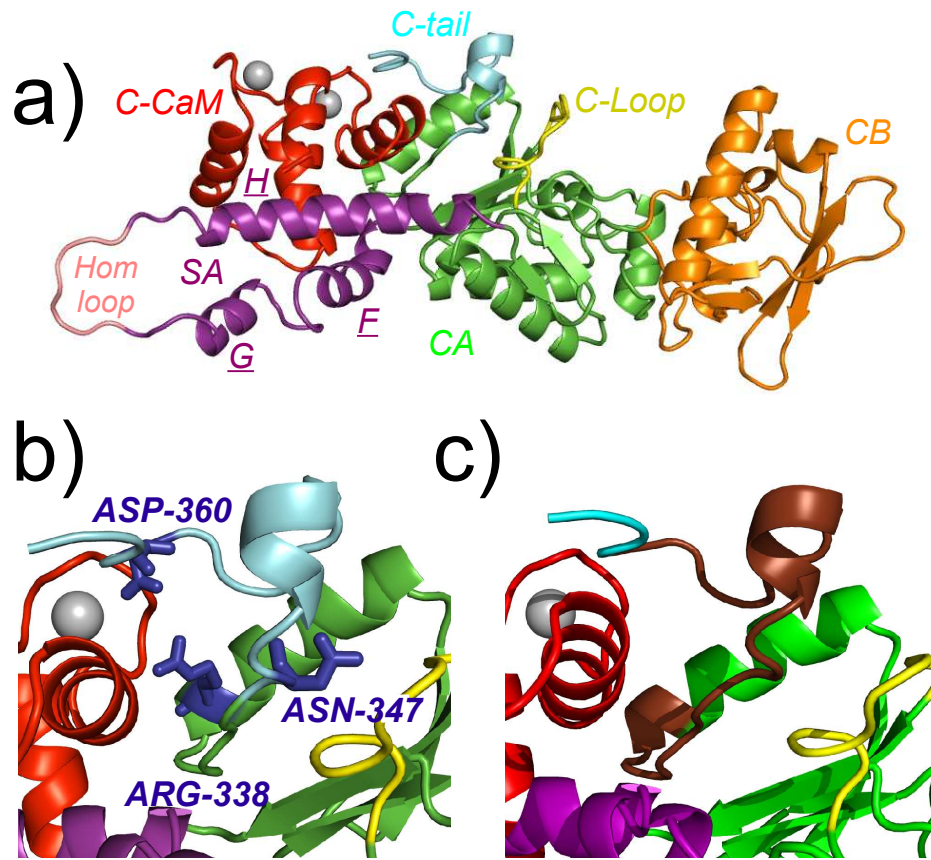


Figure 1

Figure 2

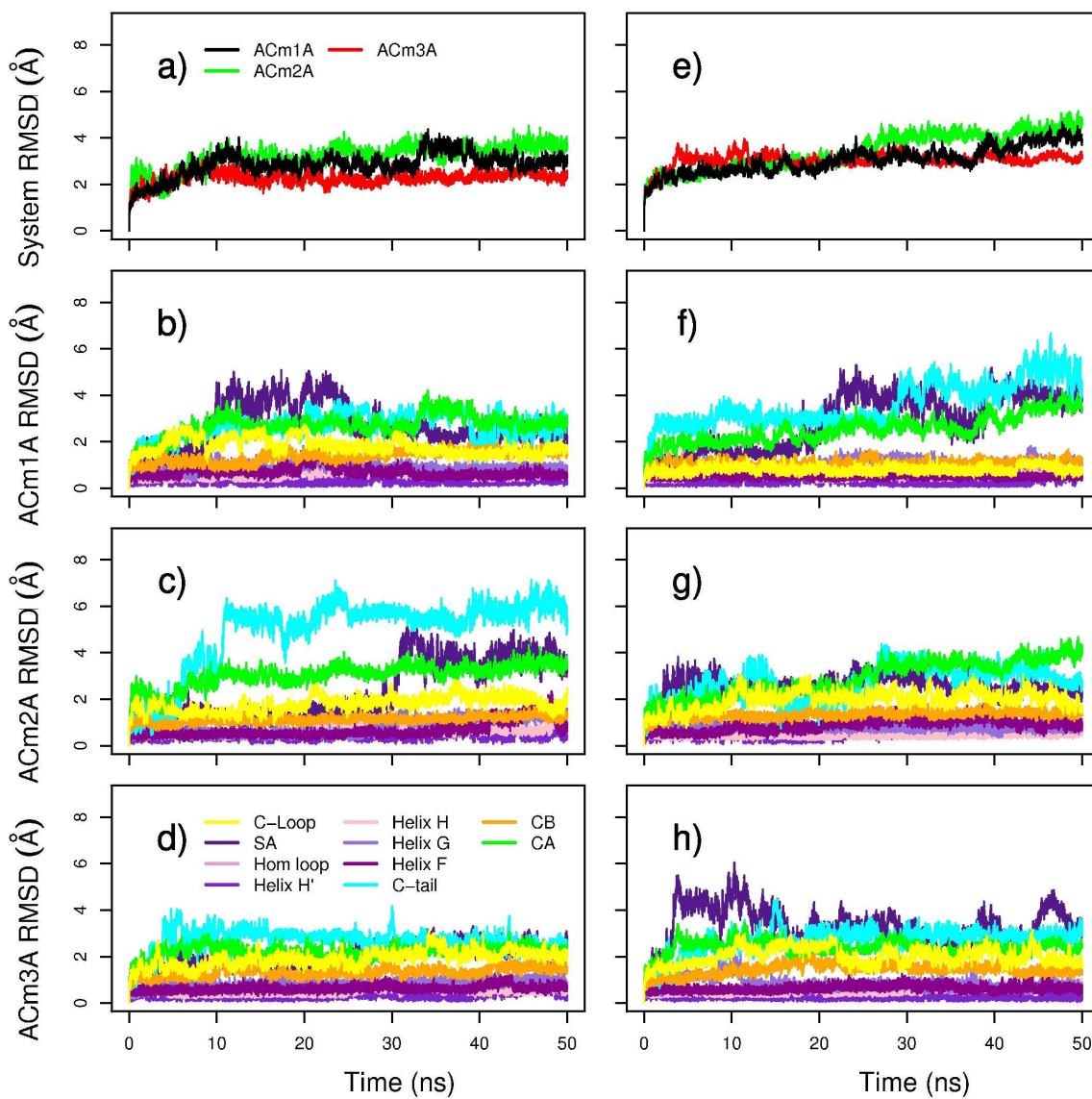


Figure 2

Figure 3

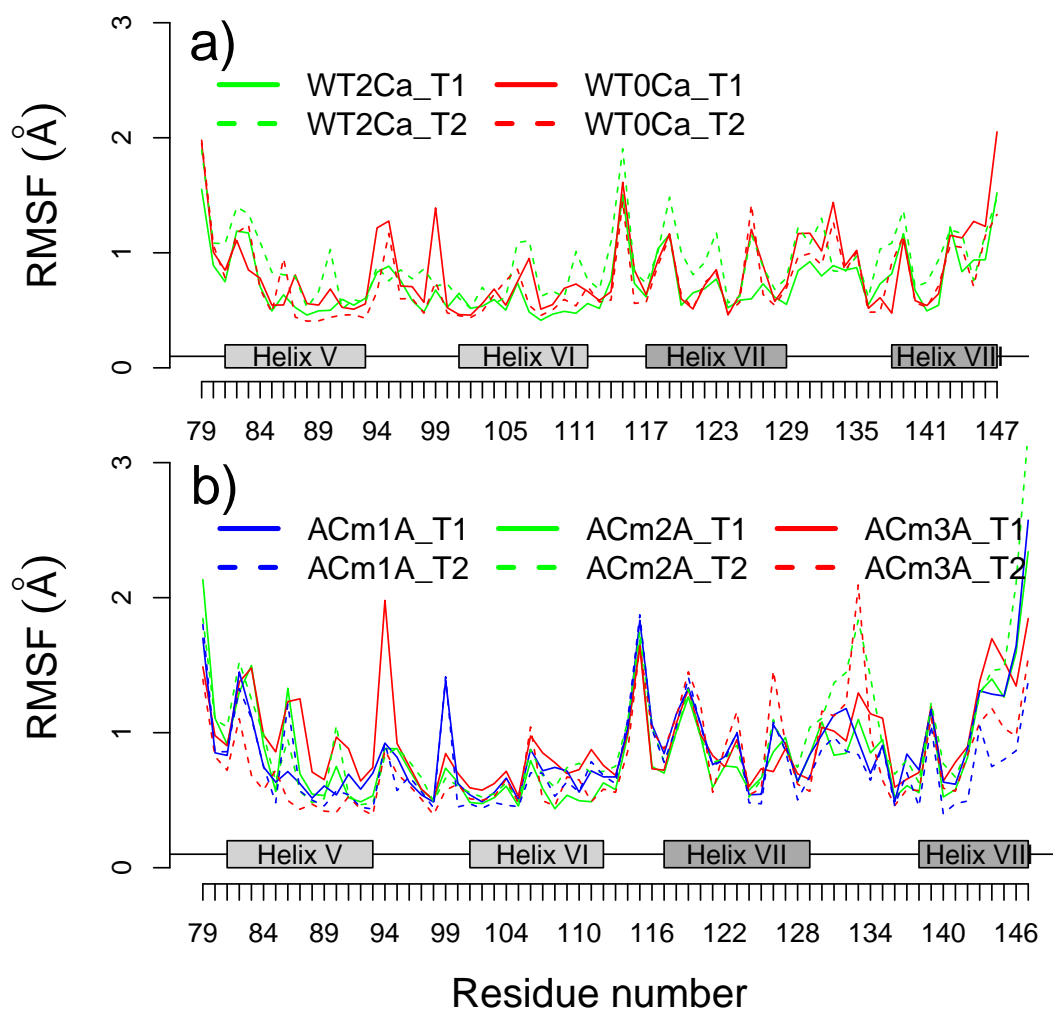


Figure 3

Figure 4

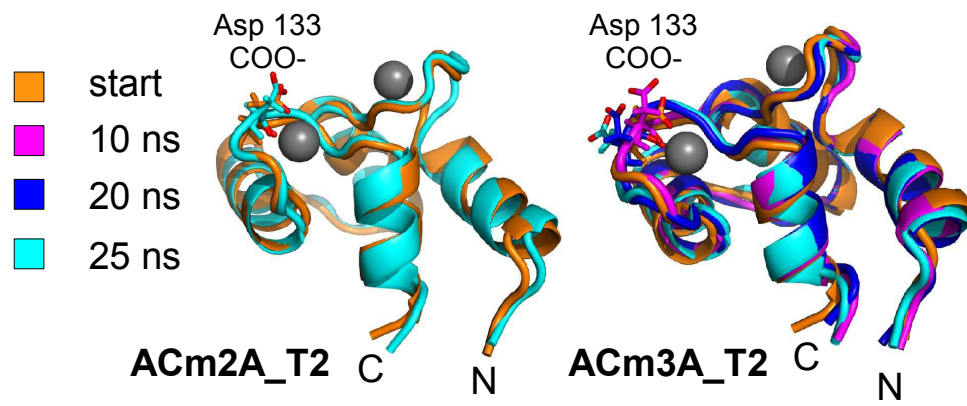


Figure 4

Figure 5

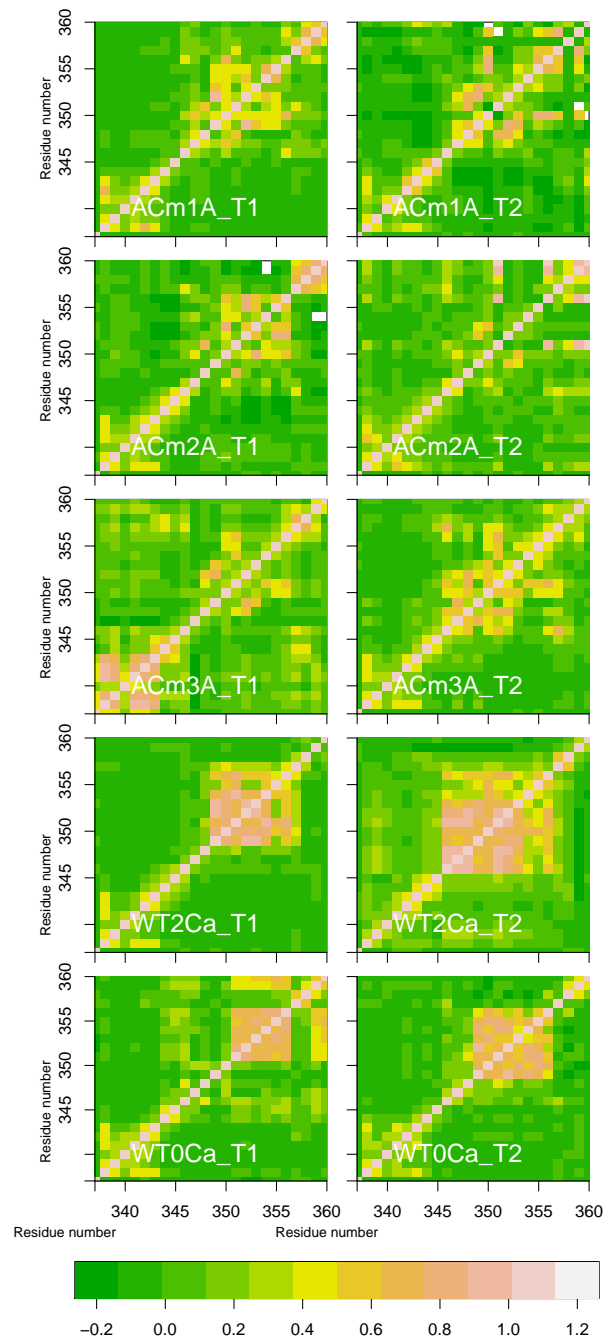


Figure 5

Figure 6

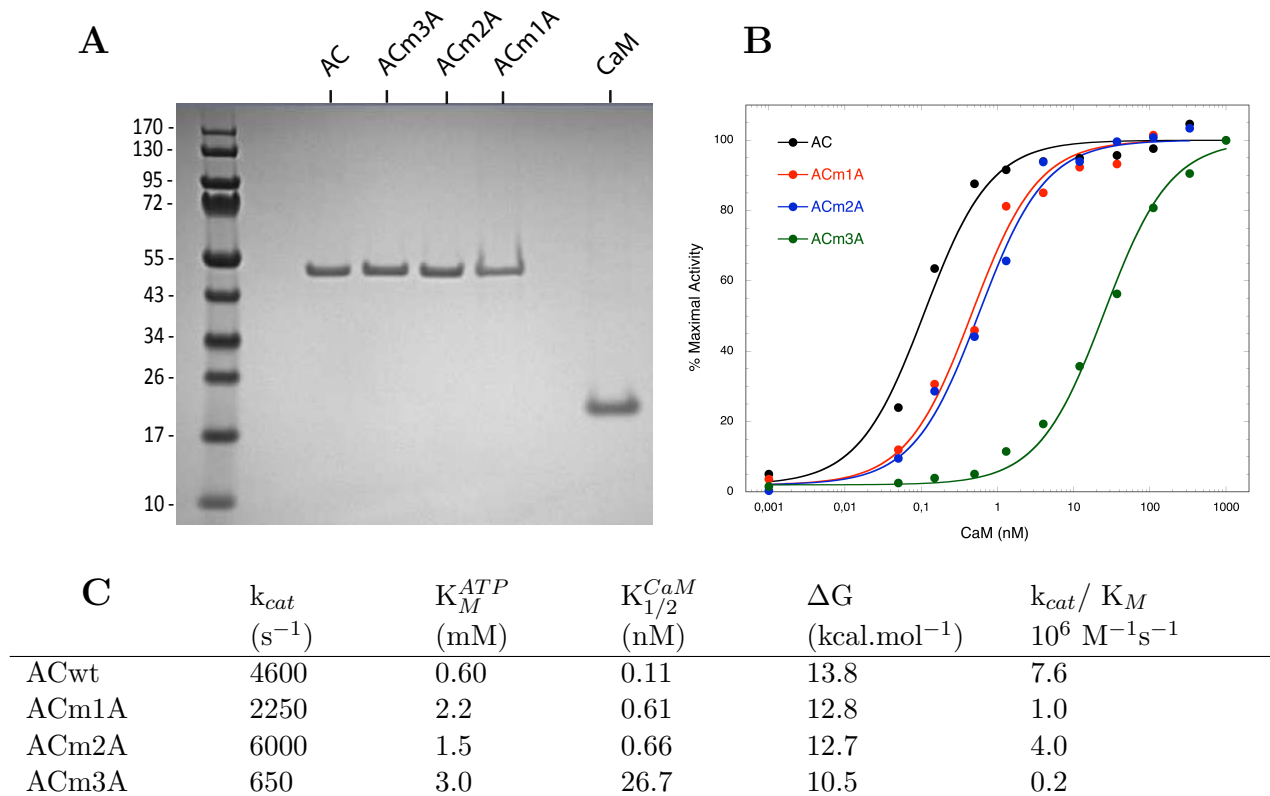


Figure 6

Figure 7

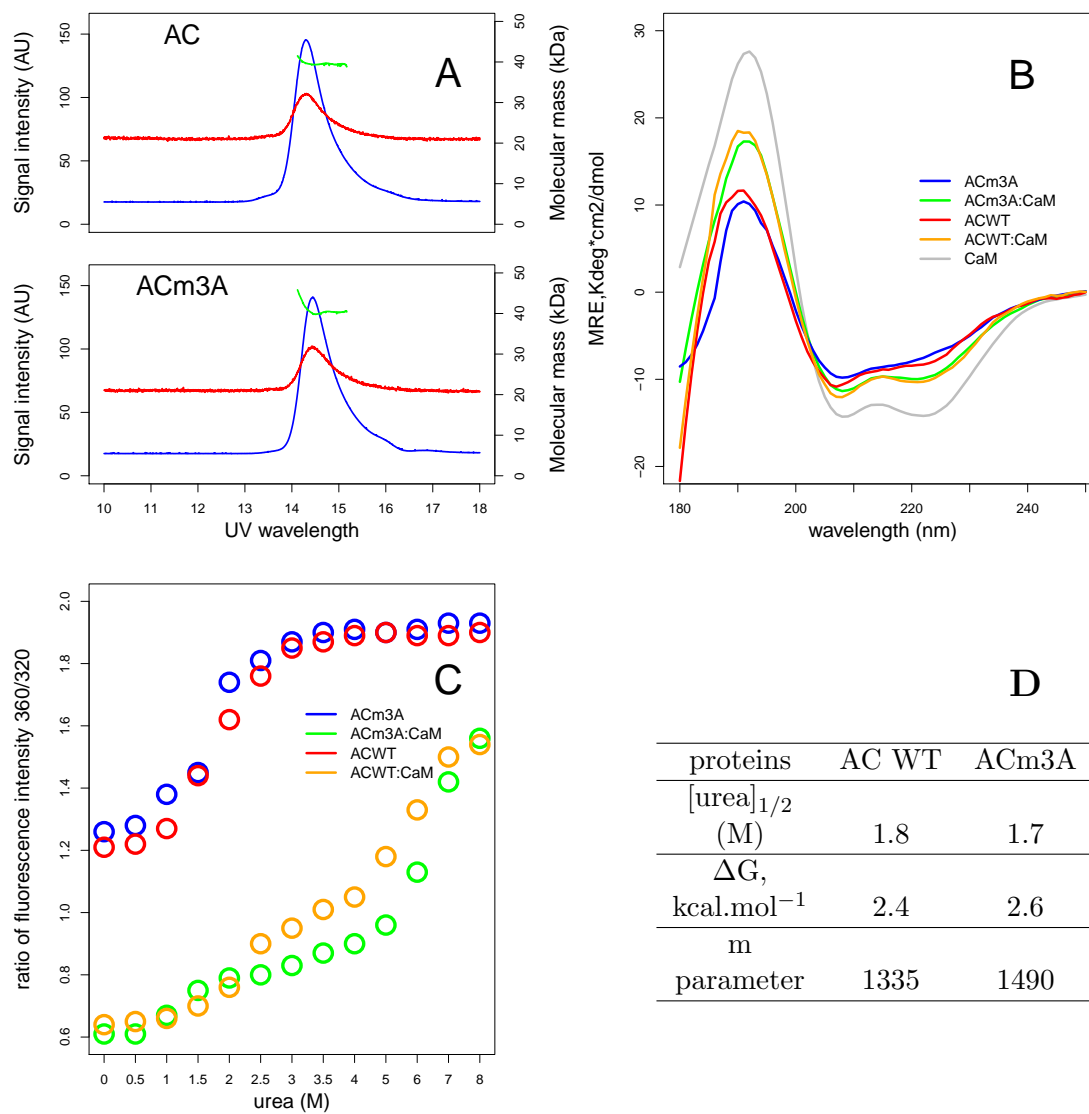


Figure 7